Acta Crystallographica Section B
Structural Science
ISSN 0108-7681

High-pressure transformations of NbO_2F

Stefan Carlson,[a]* Ann-Kristin Larsson[b] and Franziska E. Rohrer[b]

[a]ESRF, BP 220, F-38043 Grenoble CEDEX, France, and [b]Inorganic Chemistry Department, Stockholm University, S-10941 Stockholm, Sweden

Correspondence e-mail: carlson@esrf.fr

Received 13 July 1999
Accepted 25 November 1999

The ReO_3-type structure NbO_2F, niobium dioxyfluoride, has been studied at high pressures using diamond anvil cells and synchrotron X-ray radiation. High-pressure powder diffraction measurements have been performed up to 40.1 GPa. A phase transition from the cubic ($Pm\bar{3}m$) ambient pressure structure to a rhombohedral ($R\bar{3}c$) structure at 0.47 GPa has been observed. Rietveld refinements at 1.38, 1.96, 3.20, 6.23, 9.00 and 10.5 GPa showed that the transition involves an $a^-a^-a^-$ tilting of the cation–anion coordination octahedra and a change of the anion–anion arrangement to approach hexagonal close packing. Compression and distortion of the $Nb(O/F)_6$ octahedra is also revealed by the Rietveld refinements. At 17–18 GPa, the diffraction pattern disappears and the structure becomes *X*-ray amorphous.

1. Introduction

The compound NbO_2F belongs to the pseudo-binary system Nb_2O_5–NbF_5. The end members of the series are rather different compounds. In the solid state, NbF_5 consists of tetrameric Nb_4F_{20} units arranged to roughly yield a close-packed assembly of F atoms, while Nb_2O_5 exists in a number of different forms, all slab, block or columnar crystallographic shear (*CS*) derivatives of the ReO_3 structure. The oxygen-rich part of the pseudo-binary system shows several interesting structures: NbO_2F (Frevel & Rinn, 1956); Nb_3O_7F, a slab *CS* derivative of ReO_3 (Andersson, 1964); $Nb_5O_{12}F$, an incommensurately modulated structure (Larsson & Rohrer, 1999) closely related to $Ta_2O_5{\cdot}xWO_3$ (Rea *et al.*, 1995). The higher oxyfluorides in the series, *i.e.* $Nb_{17}O_{42}F$ and $Nb_{31}O_{77}F$ (Andersson, 1965; Åström, 1966) are again block *CS* derivatives of ReO_3, but contain a small amount of tetrahedrally coordinated Nb.

At ambient conditions NbO_2F has the ReO_3-type structure, showing perfect cubic symmetry (space group: $Pm\bar{3}m$) as in an undistorted ABO_3 perovskite structure with the *A* sites empty. The O and F atoms share the same crystallographic position in the structure, statistically occupied according to the stoichiometry. In general, high-pressure studies of ReO_3-type structures are of interest owing to the possibilities for the structural framework to accommodate increased pressures by *e.g.* cooperative rotation of metal–oxygen octahedra. Several authors (Razavi *et al.*, 1978; Schirber & Morosin, 1979; Schirber & Mattheiss, 1981; Batlogg *et al.*, 1984; Schirber *et al.*, 1984; Axe *et al.*, 1985; Jørgensen *et al.*, 1986; Sowa, 1988) have previously performed high-pressure investigations of ReO_3, while NbO_2F has not been studied at elevated pressures.

As derived by Glazer (1972) and recently investigated in detail by Woodward (1997), transitions in perovskite-type

structures can be described by different polyhedral tilt systems. It is reasonable to expect that pressure-induced displacive transitions by polyhedral tilts maintain the sphere-packing type for the anions. This condition is achieved for two of the tilt systems (Sowa & Ahsbahs, 1998). In the first system, $a^+a^+a^+$ using Glazer's notation (Glazer, 1972), the deformation of the sphere packing for an octahedral rotation around all cubic triad axes leads to a transformation of the space-group symmetry $Pm\bar{3}m$ to the subgroup $Im\bar{3}$ (Fisher, 1973). This transformation has been observed in ReO_3 at elevated pressures (Jørgensen *et al.*, 1986; Sowa, 1988). In the second tilt system, $a^-a^-a^-$, octahedral rotations around only one of the triad axes are allowed. This leads to the transformation from cubic symmetry to the rhombohedral symmetry $R\bar{3}c$ (VF_3-type structure). A detailed description of the group/subgroup relationship and the rotations of the octahedra have previously been given by Sowa (1997). High-temperature modifications of AF_3 (A = Al, Cr, Fe, Ga, In, Ti, V; Ravez *et al.*, 1984; Mogus-Milankovic *et al.*, 1985; Daniel *et al.*, 1990) have been shown to exhibit the cubic ReO_3-type structure, while their low-temperature structures belong to the rhombohedral VF_3-type. Recently, a high-pressure investigation of octahedron strain and rotations were performed on TiF_3 and FeF_3 (Sowa & Ahsbahs, 1998), which have structures that are very similar to the ReO_3-type at ambient conditions. It was shown that during compression the packing of the anions deforms toward a hexagonal close-packed arrangement and that repulsive interactions between cations probably induce distortions of the metal–fluorine octahedra.

The purpose of the present investigation was to examine the mixed oxygen–fluorine compound NbO_2F at high pressures and to determine if its octahedral rotations follow one of the two tilt systems, $a^+a^+a^+$ or $a^-a^-a^-$.

2. Experimental

2.1. High-pressure technique

Crystalline specimens of NbO_2F were synthesized according to Frevel & Rinn (1956). Guinier X-ray powder diffraction patterns from the powdered samples were identical to the pattern calculated from the data given in the previously published investigation (Frevel & Rinn, 1956). The unit-cell dimensions of the powders, obtained by least-squares analysis of the diffraction line positions, deviated less than 2σ from the published ones.

Membrane-driven diamond anvil cells (Letoullec *et al.*, 1988) with 300 and 600 μm diamond tip diameters were used in the high-pressure studies. Stainless steel gaskets with initial thickness of 250 μm were pre-indented to 30–60 μm. Using spark erosion (Betsa, Micro Hole 20), holes of 125 and 250 μm were made for the smaller and larger diamond tip diameters, respectively. Cryogenically loaded nitrogen and a mixture of methanol–ethanol (4/1) were used as hydrostatic compression fluids. Pressure was derived from the laser-induced (Coherent, Inova 70–2, Ar-ion laser) fluorescence of small ruby crystals (< 5 μm) located in proximity to the specimen. The wavelength shifts of the ruby R_1 fluorescence line at 694.1 nm were monitored using a computer-controlled spectrograph equipped with an array detector (Hamatsu, C5809). A linear shift was assumed to be valid within the studied pressure range and the proportionality constant 2.74 GPa nm^{-1}, derived by Piermarini *et al.* (1975), was used. Estimates of the standard deviations in the pressure determinations were obtained by combining the estimated error in the read-out of the wavelength shift (0.01 nm) with the reported e.s.d. of the proportionality constant (0.016 GPa nm^{-1}). Pressure monitoring before and immediately after the exposures ensured that changes in pressure during data collection were negligible.

2.2. Synchrotron X-ray studies

The diffraction experiments were carried out at the high-pressure beamline, ID30, European Synchrotron Radiation Facility (ESRF). Monochromatic radiation for three experiments were selected at two energies, 29.200 (0.4246 Å) and 33.169 keV (0.3738 Å), respectively. The 111 channel-cut Si monochromator, operated in a vacuum (water-cooled), was irradiated by synchrotron radiation from two phased undula-

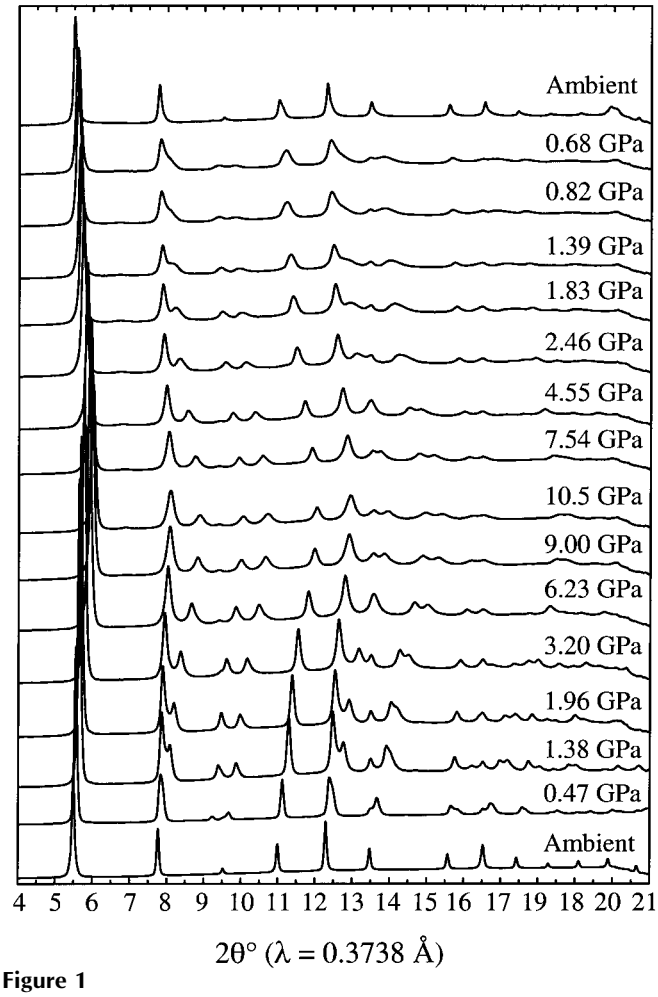

Figure 1
Diffraction patterns of the first loading of NbO_2F, using methanol–ethanol as a pressure-transmitting medium. The figure should be viewed going from the lower pattern and up. Pressure was increased to 10.5 GPa and then decreased to ambient conditions.

tors of 35 and 40 mm periods. The X-ray beam, with initial size 0.2×0.2 mm^2 after the monochromator and primary slits, was focused down to a FWHM (full-width half maximum) of 0.010×0.012 mm^2 using two bent mirrors (Yang *et al.*, 1995). This gave an effective (with tails) beam-spot size of 0.025×0.030 mm^2.

Images of the powder diffraction rings were collected with an image-plate detector (Thoms *et al.*, 1998), placed 300–400 mm from the sample. The image-plate size was 240×300 mm^2 and the pixel size $\sim 0.08 \times 0.08$ mm^2. The aperture of the diamond cell limits the data collection to 2θ angles $< 23^\circ$, so a maximum resolution of ~ 1.2 Å at the selected wavelengths could be achieved. The images were corrected for spatial distortion and non-linear features in the background and subsequently integrated over the entire powder rings, using the *FIT2D* software (Hammersley, 1998).

3. Results

As indicated above, three different loading of the DACs were performed with data collected at two wavelengths. The first loading was performed with a pressure medium of methanol–ethanol (4:1) with radiation at $\lambda = 0.3738$ Å. For the second ($\lambda = 0.4246$ Å) and third loading ($\lambda = 0.3738$ Å) N_2 was utilized as a pressure transmitting medium. The second loading was not entirely successful, resulting in non-hydrostatic conditions. Consequently, the diffraction data from that experiment is mainly given in the supplementary information.[1] Figs. 1 and 2 show the diffraction patterns from the first and third experiments on NbO_2F. The structure transforms from the cubic phase to a rhombohedral high-pressure phase already at modest pressures, as can be seen in the lower part (0.47 and 1.38 GPa) of Fig. 1. The splitting of some of the cubic peaks is also apparent in the diffraction pattern at 0.36 GPa in Fig. 2. The change from cubic symmetry to a space group compatible with the diffraction patterns of the high-pressure phase was analysed using the auto-indexing program *TREOR*97 (Werner *et al.*, 1985), powder-pattern modelling in *PowderCell*1.0 *for Windows* (Kraus & Nolze, 1997) and Rietveld refinements in *GSAS* (Larson & Von Dreele, 1994). Already in the first stages of the symmetry analysis, by comparing calculated and observed diffraction patterns, the transformation to the cubic symmetry $Im\bar{3}$ could be ruled out. Two possible space group symmetries could be imposed on the high-pressure data, up to 19.6 GPa: $R\bar{3}m$ and $R\bar{3}m$ symmetry would not display tilts of the octahedra, while a structure with $R\bar{3}c$ symmetry would have a tilt about a [111] direction of the original cubic cell. The repeat distance in all pseudo-cubic directions for a structure with $R\bar{3}c$ symmetry compared to one with $R\bar{3}m$ symmetry would therefore be doubled. The presence of $00l$ reflections with $l = 6n$ distinguish between the two space groups. Thus, $R\bar{3}c$ is the highest symmetry that is compatible with the diffraction patterns. The phase transformation from cubic to rhombohedral symmetry is reversible, as the cubic phase is recovered when returning to ambient conditions (upper pattern, Fig. 1). The asymmetry of the cubic peaks clearly indicates that some high-pressure phase still remains. Thus, the transition displays a fairly large hysteresis width extending from ~ 0.4 GPa to ambient pressure. Furthermore, this indicates a possible first-order character of the transition. In Fig. 2 a fairly sharp crystalline to *X*-ray amorphous transition can be seen at 18.5–20.8 GPa. The remaining diffraction peaks in the diagrams above 18.5 GPa are due to ε-N_2. This amorphization is quite sensitive to a non-hydrostatic condition, as the data of the second loading show indications of this transition already at 9.23 GPa. In fact, two peaks indicative of the high-pressure amorphization are visible already at 10.5 GPa in Figs. 1 and 5(*b*) ($2\theta = 5.7$ and 6.8°) showing that non-hydrostatic effects are present in the methanol–ethanol mixture. It was possible to index the diffraction patterns using the rhombohedral symmetry up to 18.5 GPa. The patterns at 0.47 and above 10.5 GPa were excluded in the Rietveld refinements owing to the mixture of phases.

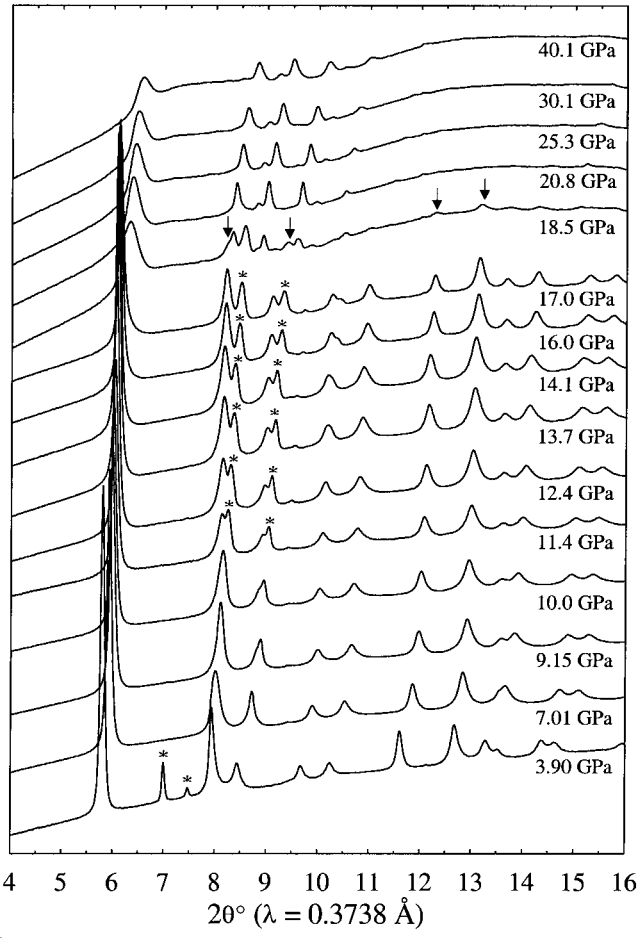

Figure 2
Diffraction patterns of the third loading of NbO_2F, using N_2 as a pressure transmitting medium. Stars indicate diffraction peaks from δ-N_2(β-N_2 at 3.90 GPa). Above 17 GPa the patterns contain mainly peaks from ε-N_2. Arrows at 18.5 GPa indicate small remaining peaks from rhombohedral NbO_2F.

[1] Supplementary data for this paper are available from the IUCr electronic archives (Reference: AD0088). Services for accessing these data are described at the back of the journal.

Table 1
Details of the high-pressure Rietveld refinements of NbO_2F, with fractional atomic coordinates, isotropic displacement parameters and selected geometrical results.

The ambient pressure data was calculated using parameters from Frevel & Rinn (1956).

P (GPa)	Ambient	1.38 (4)	1.96 (4)	3.20 (6)	6.23 (10)	9.00 (15)	10.5 (17)
d_{calc} (g cm^{-3})	3.9	4.339	4.456	4.637	4.950	5.126	5.190
No. of data		1192	1978	1978	1978	1978	1978
Observed reflections†		75	72	87	31	85	88
No. of parameters		16	17	6	17	17	17
R_p‡		0.015	0.012	0.014	0.009	0.008	0.008
wR_p§		0.023	0.020	0.020	0.013	0.011	0.012
R_F^2¶		0.082	0.071	0.040	0.056	0.047	0.052
χ^2 ††		1.08	0.78	0.84	0.33	0.26	0.25
x(O/F)‡‡	0.5	0.4232 (17)	0.4112 (9)	0.3912 (8)	0.3748 (6)	0.3674 (6)	0.3675 (7)
U_{iso}(O/F)		0.016 (3)	0.0031 (18)	0.0074 (18)	0.0143 (12)	0.0127 (13)	0.0130 (15)
U_{iso}(Nb)		0.0079 (11)	0.0266 (8)	0.0208 (5)	0.0359 (6)	0.0315 (7)	0.0302 (8)
Nb—(O/F) (Å)	6 × 1.951	4 × 1.946 (1)	4 × 1.943 (1)	4 × 1.945 (2)	4 × 1.929 (1)	4 × 1.919 (1)	4 × 1.911 (1)
		2 × 1.946 (4)	2 × 1.944 (4)	2 × 1.945 (5)	2 × 1.929 (2)	2 × 1.919 (2)	2 × 1.911 (3)
Nb—Nb (Å)	3.902	3.8061 (4)	3.7737 (3)	3.7267 (2)	3.6531 (3)	3.6154 (4)	3.6024 (5)
(O/F)—(O/F) (Å)	8 × 2.759	2 × 2.745 (6)	4 × 2.739 (6)	2 × 2.737 (5)	4 × 2.696 (6)	2 × 2.671 (4)	2 × 2.653 (4)
		2 × 2.746 (5)	2 × 2.757 (3)	2 × 2.738 (4)	2 × 2.759 (2)	2 × 2.672 (3)	2 × 2.654 (4)
		4 × 2.759 (4)	2 × 2.758 (4)	2 × 2.763 (3)	2 × 2.958 (2)	2 × 2.755 (2)	3 × 2.751 (2)
		2 × 3.290 (4)	2 × 3.119 (4)	2 × 2.764 (4)	2 × 3.211 (2)	2 × 2.756 (2)	1 × 2.752 (3)
						2 × 2.912 (2)	2 × 2.906 (2)
(O/F)—Nb—(O/F) (°)	12 × 90	6 × 89.7 (2)	6 × 89.6 (2)	6 × 89.5 (1)	6 × 88.7 (1)	6 × 88.2 (1)	6 × 87.9 (1)
	3 × 180	6 × 90.3 (2)	6 × 90.4 (2)	6 × 90.5 (1)	6 × 91.3 (1)	6 × 91.8 (1)	6 × 92.1 (1)
		3 × 180.0 (5)	3 × 180.0 (5)	3 × 180.0 (7)	3 × 180.0 (1)	3 × 180.0 (2)	3 × 180.0 (1)
Nb—(O/F)—Nb (°)	180	155.8 (3)	152.3 (3)	146.7 (2)	142.5 (2)	140.8 (2)	140.9 (2)
V_{poly}: Nb(O/F)$_6$(Å^3)	9.90	9.83 (3)	9.78 (2)	9.80 (2)	9.55 (1)	9.40 (1)	9.29 (1)

† $I_o \geq \sigma_I$. ‡ $R_{wp} = \{\Sigma w_i[y_i(\text{obs}) - y_i(\text{calc})]^2/\Sigma w_i[y_i(\text{obs})]^2\}^{1/2}$. § $R_p = \Sigma|y_i(\text{obs}) - y_i(\text{calc})|/\Sigma y_i(\text{obs})$. ¶ $R_F^2 = \Sigma|F_{hkl}(\text{obs})^2 - F_{hkl}(\text{calc})^2|/F_{hkl}(\text{obs})^2$. †† $\chi^2 = \Sigma w_i(y_i(\text{obs}) - y_i(\text{calc}))^2/(N_{obs} - N_{var})$. ‡‡ The Nb and O/F fractional coordinates are constrained by symmetry to (0,0,0) and $(x,0,\frac{1}{4})$, respectively.

For convenience, the discussions below use the hexagonal rather than the rhombohedral unit-cell parameters. The rhombohedral parameters a_r and α_r are related to the hexagonal lattice constants (Megaw & Darlington, 1975)

$$a_r = (3a_h^2 + c_h^2)^{1/2}/3 \quad (1)$$

and

$$\alpha_r = 2\sin^{-1}\{3/[2(3 + c_h^2/a_h^2)^{1/2}]\}. \quad (2)$$

The relative changes of the unit-cell parameters *versus* pressure, obtained from the profile fits in *GSAS* (Larson & Von Dreele, 1994), for the experiments on NbO_2F are shown in Fig. 3. The compression of the unit cell is very anisotropic below 18.5 GPa, with the *c*-axis remaining fairly constant and the *a*-axis decreasing by 14.8%. This anisotropy gives a rapid increase in the *c*/*a* ratio from ambient conditions to 20 GPa, as shown in Fig. 4. The solid line in Fig. 3 shows a fit of the Vinet equation-of-state (Vinet *et al.*, 1986)

$$P = 3B_0(V/V_0)^{2/3}[1 - (V/V_0)^{1/3}] \times \exp\{(3/2)(B' - 1)[1 - (V/V_0)^{1/3}]\} \quad (3)$$

to the pressure–volume data below 18.5 GPa. In (3), V is the observed unit-cell volume and V_0 is the volume at ambient conditions (constrained in the fit to 356.46 Å^3). The fitted bulk modulus at zero pressure B_0 and its pressure derivative B' became 9.6 (3) and 11.7 (3) GPa, respectively. This high compressibility (low B_0) and large curvature (high B') can sometimes be seen for other framework structures (*e.g.* $NbSbF_6$: Sowa, 1997; TiF_3 and FeF_3: Sowa & Ahsbahs, 1998), displaying rigid groups which govern the compression by tilting or other types of rearrangements between the groups. The expected value of B' would be 4, but in this case, where the compression of the unit cell is very anisotropic (only the *a*-axes are compressed), the seemingly non-physical value of 11.7 is obtained.

Rietveld refinements were performed using *GSAS* (Larson & Von Dreele, 1994) on six high-pressure diffraction patterns

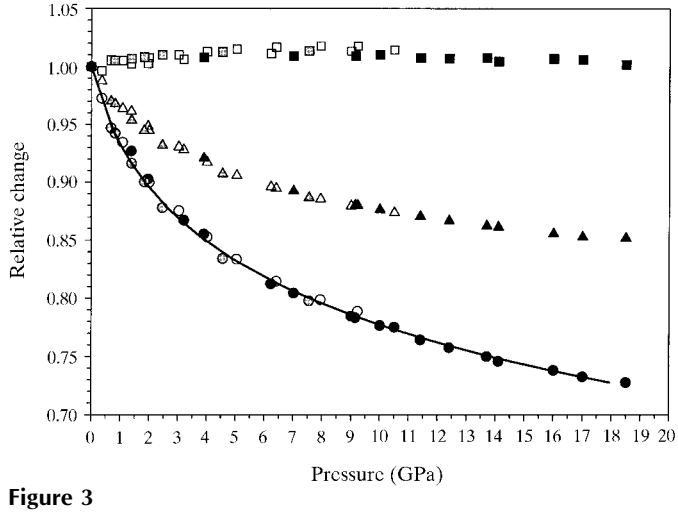

Figure 3
The relative change in the unit-cell parameters (a/a_0 triangles, c/c_0 squares, V/V_0 circles) *versus* pressure for NbO_2F. White and black markers indicate increasing pressure for the first and third loading, respectively. Grey markers indicate decreasing pressure (first loading). The solid line shows a fit of the Vinet *EOS* for the data up to 18.5 GPa. Data from the three different loading are shown.

from the first loading. Table 1 shows the detailed results of these refinements. The structural model used five parameters: a fractional coordinate for the disordered position of O and F, an isotropic displacement parameter for O/F and Nb, and unit-cell parameters. In addition, an overall scale factor and different numbers of profile and background parameters were refined. The refinements were performed until convergence was obtained ($\sum$shifts < 0.01). As can be seen from Table 1, the R_F^2 and wR_p values range from 0.040 to 0.082 and 0.011 to 0.023, respectively, indicating a reasonable agreement of the structural parameters with the observed data. The χ^2 values are anomalously low, possibly due to the combination of an increased background at higher pressures and the method of calculating e.s.d.s for the powder profile intensities. The refined isotropic displacement parameters from the high-pressure data must also be regarded with some caution, since they tend to include the possible systematic errors in the measurements, such as absorption, preferred orientation or line broadening due to non-hydrostatic conditions. Two representative difference plots resulting from the Rietveld refinements are shown in Fig. 5. The geometric calculations of bond lengths, angles and polyhedron volumes in Table 1 were performed with the programs *PLATON* (Spek, 1990) and *VOLCAL* (Finger, 1971), respectively. The structure diagrams described below were made using the program *ATOMS* (Dowty, 1989).

4. Discussion

An illustration of the pressure-induced topological changes of the corner-connected $Nb(O/F)_6$ octahedral network in NbO_2F is shown in Fig. 6. As indicated above, the structure has already transformed from cubic ($Pm\bar{3}m$) to rhombohedral ($R\bar{3}c$) symmetry at 0.47 GPa. This represents an $a^-a^-a^-$ change of the tilt system (in Glazer's notation) to the VF_3 structure type. As seen in the upper part of Fig. 6, the rotations around one of the triad axes of the cubic ambient structure tilts the octahedra into the empty space between them. In the lower part of Fig. 6, a projection of only two layers of the *ABABA* packing pattern of the anions is shown. The light-coloured spheres form the top layer of anions and the dark ones the lower layer, with their ionic radius set to contact with the nearest neighbouring anion. As we go up in this series of pressures (lower part of Fig. 6) to the highest pressure of 10.5 GPa, the structure gradually becomes more close-packed, approaching the hexagonal close-packing. Thus, as has previously been observed for the rigid tetrahedra of *e.g.* α-quartz (Hazen *et al.*, 1989), we see directly from Fig. 6 that the reduction of the volume between the rigid octahedra is accompanied by a greater anion packing efficiency under compression.

Harmonic average values, $d_{av} = \{[1/n\sum(1/d_{anion})^2]^{-1}\}^{1/2}$, calculated from the (O/F)—(O/F) distances in Table 1 are plotted *versus* applied pressure in Fig. 7. The unfilled markers are the average distances calculated using the eight nearest anion neighbours, which corresponds to the cubic ambient pressure structure. The filled markers were calculated from ten anion–anion distances below 3 Å, thereby including a higher coordination number for the anions. The average

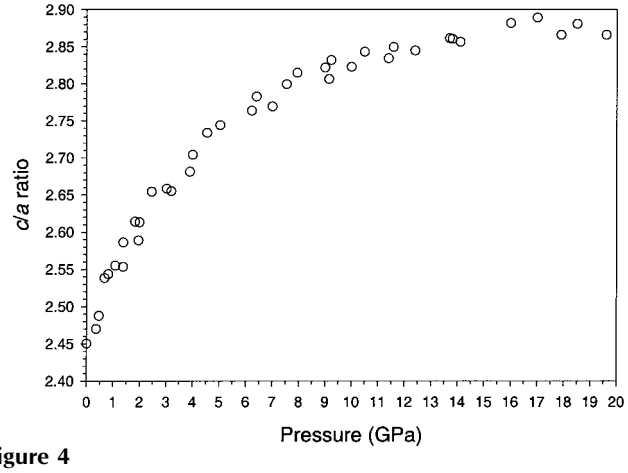

Figure 4
The *c*/*a* ratio *versus* pressure for NbO_2F. Data from the three different loadings are shown.

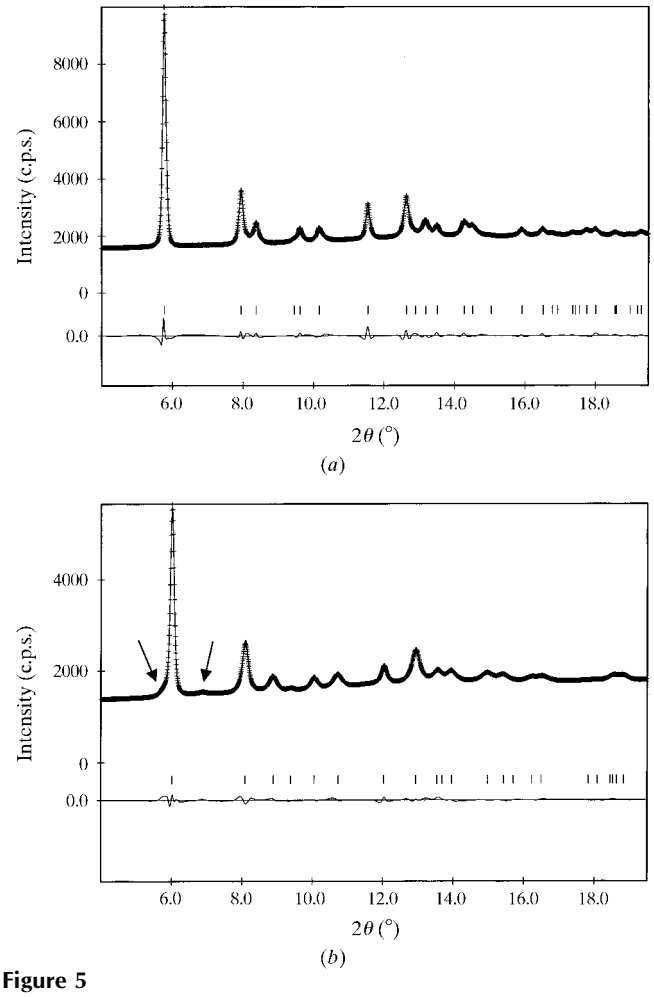

Figure 5
Representative difference plots from Rietveld refinements of the rhombohedral high-pressure phase of NbO_2F at (*a*) 3.20 and (*b*) 10.5 GPa. The allowed reflections of $R\bar{3}c$ are indicated with tick marks. Observed and calculated points are given as (+) and (−), respectively. The difference plot is shown below the tick marks.

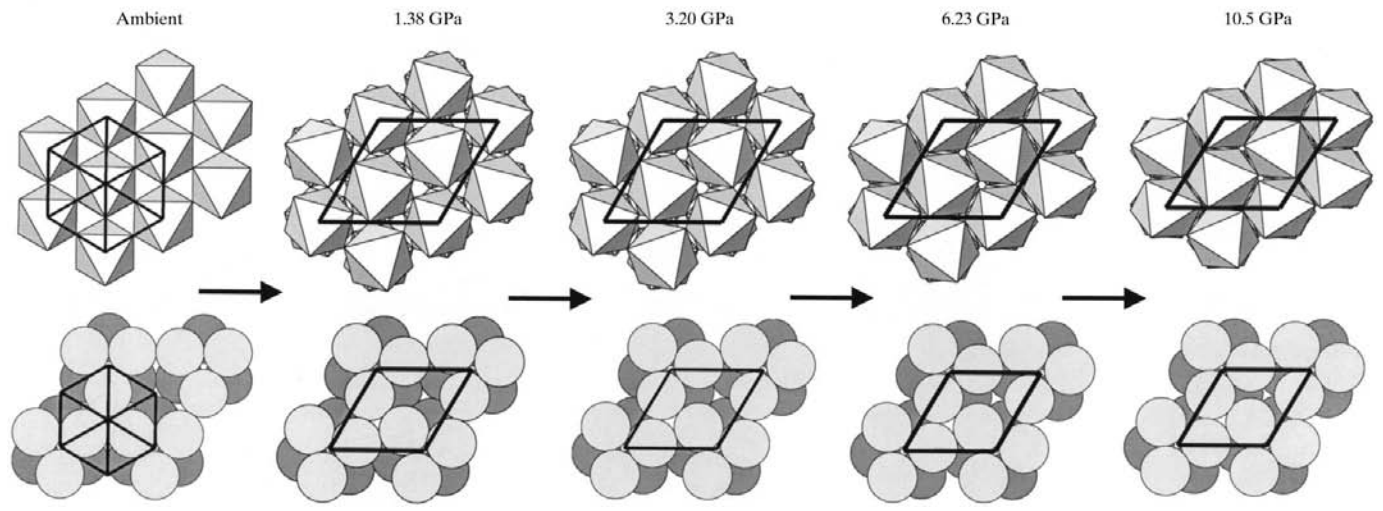

Figure 6
Illustration of the compression of the NbO_2F structure from ambient pressure to 10.5 GPa. The octahedra represent the sixfold coordination of O and F around Nb. For comparison, the ambient pressure phase (cubic) is shown along [111], while the rhombohedral phase is shown along the [001] direction, in the hexagonal setting.

distances for 8 and 10 neighbours, respectively, may be fitted by the linear equations

$$d_{\rm av}(8) = 2.840 - 0.0101P \quad (4)$$

and

$$d_{\rm av}(10) = 2.761 - 0.0055P. \quad (5)$$

By assuming a linear decrease of the average anion–anion distances from ambient pressure to 20 GPa (dashed lines in Fig. 7), an extrapolation of the data would give the hexagonal close-packing with an anion–anion distance of 2.67 Å at 17.5 GPa. This corresponds quite closely to the pressure where the structure becomes X-ray amorphous (Fig. 2).

These observations indicate that the repulsive interactions between anions are the major reason for the cubic to rhombohedral transition at low pressures. At higher pressures the situation becomes more complicated as a perfect hexagonal close-packing of anions is hindered by cation–cation and cation–anion interactions. One might speculate that the incompatibility of the hexagonal close-packing of the anions with the packing of the cations is responsible for the loss of long-range order, showed by the apparent pressure-induced amorphization above 18.5 GPa (Fig. 2).

The transition from $Pm\bar{3}m$ to $R\bar{3}c$ seems to be of displacive character. A way of analysing displacive transitions is using Landau's theory of continuous phase transitions (Landau & Lifshitz, 1980). Landau postulated that the excess entropy owing to a phase transition is proportional to Q^2, where Q is the order parameter. Following the discussion of Carpenter (1992), the excess free energy at a constant temperature can be described as

$$G = 1/2a_v(P - P_c)Q^2 + 1/4bQ^4 + ..., \quad (6)$$

where P_c is the critical pressure for the transition, while a_v and b are coefficients in the series expansion with the subscript v indicating units of volume.

For two phases at equilibrium the condition is $\delta G/\delta Q = 0$ giving

$$Q = [a_v/b(P_c - P)]^{\beta}. \quad (7)$$

A value of the critical coefficient $\beta = \frac{1}{2}$ implies that the transitions follow mean-field theory, with small fluctuations in the order parameter, and can thus be analysed using Landau theory. In the case of a coefficient $\beta = \frac{1}{4}$ the transition is said to be tricritical, which represents an intermediate stage between first- and second-order transitions. An appropriate order parameter for the displacive transitions in ReO_3 (Jørgensen *et al.*, 1986) and compounds with $R\bar{3}c$ symmetry (Michel *et al.*, 1971) has been shown to be the rotation angle (ω) around the triad axes of the octahedra. The rotation angle can be expressed in two ways (Michel *et al.*, 1971). Assuming that no

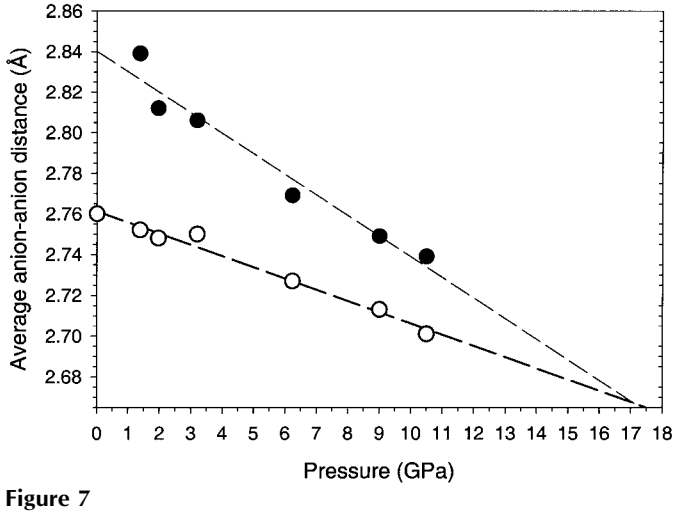

Figure 7
Harmonic average values for the (O/F)—(O/F) distances in NbO_2F *versus* pressure. The unfilled and filled markers are the average distances calculated using 8 and 10 nearest anion neighbours, respectively. The dashed lines are linear least-squares fits to the data.

distortions of the $Nb(O/F)_6$ octahedra occur, ω can be calculated from the c/a ratio of the hexagonal unit-cell

$$\omega = \cos^{-1}[6^{1/2}/(c/a)]. \quad (8)$$

If the distortions are also to be included, the calculation has to be made from the fractional coordinates x(O/F)

$$\omega = \tan^{-1}[2(3)^{1/2}(1/2 - x(O/F))]. \quad (9)$$

Jørgensen *et al.* (1986) used a power law of the form

$$\omega \propto (P - P_c)^{\beta}, \quad (10)$$

which was fitted to the ω data for ReO_3, yielding a value of β = 0.322 (5). In Fig. 8 the variation of ω *versus* applied pressure is shown. The unfilled and filled markers represent ω calculated from (8) and (9), respectively. The solid lines are fits of the power law (10) to the rotation angles, resulting in the values P_c = 0.35 (1) and 1.1 (2) GPa, and β = 0.21 (1) and 0.14 (2) for the data calculated using (8) and (9), respectively. The values of β indicate a first-order or tricritical phase transition, with a large critical region (more than 24°) for the rotation angle. From Fig. 8 it is also apparent that the rotation angle has to be calculated from the refined atomic positions, since otherwise the angle is overestimated by 6–7° at the highest pressures, using the c/a ratio. The fact that P_c [c/a] is lower than $P_c[x(O/F)]$ could indicate a second phase transition at very low pressures. A transition to *e.g.* $R\bar{3}m$ would leave x(O/F) invariant at $\frac{1}{2}$, 0, $\frac{1}{2}$ and allow the c/a ratio to change. More detailed experiments in the pressure range from ambient to 0.5 GPa has to be made to resolve this matter.

As indicated above, the compression mechanism of NbO_2F does not only involve tilting of the $Nb(O/F)_6$ octahedra, but also compression of Nb—(O/F) bonding distances within the octahedra. The polyhedral volume $V_{poly}[Nb(O/F)_6]$ in Table 1 decreases ~6% when increasing the pressure from ambient conditions to 10.5 GPa. This change in polyhedral volume is accompanied by a 2% decrease of the Nb—(O/F) distance and a slight distortion of the $Nb(O/F)_6$ octahedra, which can be seen from the variation of the (O/F)—Nb—(O/F) angles with pressure (Table 1). From the 90° angles in the $Nb(O/F)_6$ octahedron at ambient conditions, a split (by symmetry) into two different angles can be observed after the phase transition. At the highest pressure (10.5 GPa) a deviation of 2.1° occurred. These results show that the compression of the high-pressure phase of NbO_2F cannot be described only in terms of polyhedral tilts, but also changes in cation–anion distances have to be taken into account. This fact has previously been discussed by *e.g.* Sowa & Ahsbahs (1998) for pressure-induced octahedron strain in VF_3-type compounds.

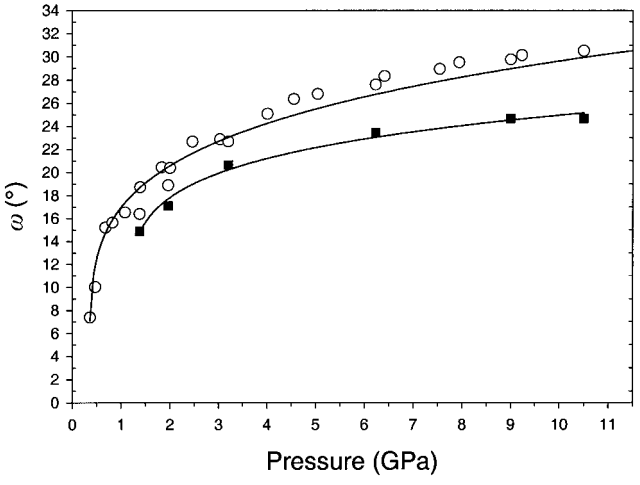

Figure 8
Rotation angle ω *versus* pressure. Unfilled and filled markers were calculated using the c/a ratio and x(O/F), respectively. The solid lines represent fits to the power law $\omega = (P - P_c)^{\beta}$.

5. Conclusions

A high-pressure displacive transition from cubic ($Pm\bar{3}m$) to rhombohedral ($R\bar{3}c$) symmetry between ambient pressure and 0.47 GPa has been observed for NbO_2F. The change of the anion arrangement towards hexagonal close-packing and $a^-a^-a^-$-type tilting (in Glazer's notation) of the $Nb(O/F)_6$ octahedra seems to be the major adjustment of the structure to the applied pressure. The transition is fully reversible, showing a slight hysteresis. The critical exponent β derived using Landau's theory of continuos phase transitions indicates a first or tricritical order for the transition. At 18.5 GPa, a second high-pressure transformation was observed that makes NbO_2F X-ray amorphous. This transition can be anticipated to also involve the cation–anion interactions, seen from the pressure-induced distortions of the $Nb(O/F)_6$ octahedra.

The authors are grateful for the kind help by technician Stany Bauchau, Dr Tristan Le Bihan and Dr Mohamed Mezouar at beamline ID30, ESRF.

References

Andersson, S. (1964). *Acta Chem. Scand.* **18**, 2339–2344.
Andersson, S. (1965). *Acta Chem. Scand.* **19**, 1401–1404.
Åström, A. (1966). *Acta Chem. Scand.* **20**, 969–982.
Axe, J. D., Fujii, Y., Batlogg, B., Greenblatt, M. & Di Gregorio, S. (1985). *Phys. Rev. B*, **31**, 663–667.
Batlogg, B., Maines, R. G., Greenblatt, M. & Di Gregorio, S. (1984). *Phys. Rev. B*, **29**, 3762–3764.
Carpenter, M. A. (1992). *The Stability of Minerals.* The Mineralogy Society Series 3, edited by G. D. Price and N. L. Ross, pp. 181–184. London: Chapman and Hall.
Daniel, P., Bolou, A., Rousseau, M., Nouet, J. & Leblanc, M. (1990). *Phys. Rev. B*, **42**, 10545–10552.
Dowty, E. (1989). *ATOMS.* Dowty, 521 Hidden Valley Road Kingsport, TN 37663, USA.
Finger, L. W. (1971). *VOLCAL.* Carnegie Institute of Washington, Geophysical Laboratory, Washington DC, USA.
Fisher, W. (1973). *Z. Kristallogr.* **138**, 129–146.
Frevel, L. K. & Rinn, H. W. (1956). *Acta Cryst.* **9**, 626–627.
Glazer, A. M. (1972). *Acta Cryst.* B**28**, 3384–3392.
Hammersley A. (1998). *FIT2D V10.3 Reference Manual V4.0*. ESRF, Grenoble, France.
Hazen, R. M., Finger, L. W., Hemley, R. J. & Mao, H. K. (1989). *Solid State Commun.* **72**, 507–511.
Jørgensen, J. E., Jorgensen, J. D., Batlogg, B., Remeika, J. P. & Axe, J. D. (1986). *Phys. Rev. B*, **33**, 4793–4798.

Kraus, W. & Nolze, G. (1997). *PowderCell for Windows*, Version 1.0. Federal Institute for Materials, Research and Testing, Berlin, Germany.
Landau, L. D. & Lifshitz, E. M. (1980). *Statistical Physics*. Oxford: Pergamon Press.
Larson, A. C. & Von Dreele, R. B. (1994). LANSCE MS-H805. Los Alamos National Laboratory, Los Alamos, USA.
Larsson, A.-K. & Rohrer, F. E. (1999). Private communication.
Letoullec, R., Pinceaux, J. P. & Loubeyre, P. (1988). *High Press. Res.* **1**, 77–90.
Megaw, H. D. & Darlington, C. N. W. (1975). *Acta Cryst.* A**31**, 161–173.
Michel, C., Moreau, J. M. & James, W. J. (1971). *Acta Cryst.* B**27**, 501–503.
Mogus-Milankovic, A., Ravez, J., Chaminade, J. P. & Hagenmuller, P. (1985). *Mater. Res. Bull.* **20**, 9–17.
Piermarini, G. J., Block, S., Barnett, J. D. & Forman, R. A. (1975). *J. Appl. Phys.* **46**, 2774–2780.
Ravez, J., Mogus-Milankovic, A., Chaminade, J. P. & Hagenmuller, P. (1984). *Mater. Res. Bull.* **19**, 1311–1316.
Razavi, F. S., Altounian, Z. & Datars, W. R. (1978). *Solid State Commun.* **28**, 217–220.
Rea, D., Schmid, S., Thompson, J. G. & Withers, R. (1995). *Acta Cryst.* B**51**, 709–721.
Schirber, J. E. & Mattheiss, L. F. (1981). *Phys. Rev. B*, **24**, 692–697.
Schirber, J. E. & Morosin, B. (1979). *Phys. Rev. Lett.* **42**, 1485–1487.
Schirber, J. E., Morosin, B., Alkair, R. W., Larson, A. C. & Vergamini, P. J. (1984). *Phys. Rev. B*, **29**, 4150–4152.
Sowa, H. (1988). *Z. Kristallogr.* **184**, 257–268.
Sowa, H. (1997). *Acta Cryst.* B**53**, 25–31.
Sowa, H. & Ahsbahs, H. (1998). *Acta Cryst.* B**54**, 578–584.
Spek, A. L. (1990). *PLATON*. University of Utrecht, The Netherlands.
Thoms, M., Bauchau, S., Hausermann, D., Kunz, M., Le Bihan, T., Mezouar, M. & Strawbridge, D. (1998). *Nucl. Instrum. Methods Phys. Res. A*, **413**, 175–184.
Vinet, P., Ferrante, J., Smith, J. R. & Rose, J. H. (1986). *J. Phys. C*, **19**, L467–L473.
Werner, P.-E., Eriksson, L. & Westdahl, M. (1985). *J. Appl. Cryst.* **18**, 367–370.
Woodward, P. M. (1997). *Acta Cryst.* B**53**, 32–43.
Yang, B. X., Rivers, M., Schildkamp, W. & Eng, P. J. (1995). *Rev. Sci. Instrum.* **66**, 2278–2280.